Curvature related Eddy current losses in laminated Axial flux machine cores.

A. Ahfock and A. J. Hewitt MIEE.

Abstract — In this paper we present an axiperiodic quasi-static model to evaluate the magnetic flux density distribution and power loss due to curvature related radial flux in the laminated core of axial flux machines. It is shown that the relatively low effective permeability in the radial direction and the shielding effect of induced eddy currents result in negligible radial flux density compared to the peak flux densities in the axial and circumferential directions. This justifies the assumption of zero radial flux which simplifies electromagnetic modelling of axial flux machine cores. The model predicts that power loss due to curvature related radial flux is insignificant compared to normal eddy current loss if the core permeability, core conductivity and number of poles are sufficiently high. A laboratory technique is proposed for the practical detection of power loss due to curvature related radial flux.

Index Terms — axial flux machines, magnetic flux density distribution, axiperiodic electromagnetic model, eddy currents.

NOMENCLATURE

B = magnetic flux density
D = power loss density
E = electric field intensity
F = loss due to cross-lamination flux
f = frequency
H = magnetic field intensity
I = vector of induced currents
J = induced current density
L = core axial length
P = matrix of permeances
P = total core loss
p = number of machine poles
Q = matrix of permeances
R = matrix of resistances
R_i = core inner radius
R_o = core outer radius
S = matrix of permeances
T = electric vector potential
W = matrix of permeances

δ = skin depth
μ = material permeability
σ = material conductivity
$\mathbf{\Phi}$ = vector of imposed magnetic flux
$\mathbf{\Omega}$ = vector of magnetic scalar potentials
ω = angular frequency

I. INTRODUCTION

Axial flux machines (AFMs), because of their physical structure, have an advantage in applications such as fans, disk drives and some electric vehicles. It has also been suggested [1,2,3] that, compared to radial flux machines they have greater power to weight ratios.

It is important for those who design AFMs to have a good understanding of the magnetic flux density distribution in those machines. There have been a number of publications [2,4,5] on the flux density distribution in the air-gap of AFMs. However, they effectively ignore the flux density distribution in the iron cores since infinite permeability is assumed. In this paper the focus is on the flux distribution in the laminated cores of AFMs taking into consideration the curvature of the core. The aim is to determine the practical significance of any curvature related radial component of flux density that may be present in the core. Boldea, Rahman and Nasar [6] derive expressions for the flux density in machine cores, but they ignore the effects of curvature. Hewitt, Ahfock and Suslov [7] concluded that curvature related radial flux density is relatively small compared to the peak axial and circumferential flux densities even when the shielding effect of induced eddy currents is ignored. Their model is a magnetostatic one and thus did not address the question of power loss resulting from curvature related radial flux. In this paper a quasi-static electromagnetic model is used to confirm the findings of [7] and to evaluate power loss due to curvature related radial or cross-lamination flux. The model is specifically for cores in which the flux enters axially from the air-gap(s) and then travels circumferentially.

In Section II it is shown that power loss due to cross-lamination flux is decoupled from power loss due to parallel running flux. Therefore, their theoretical evaluations can be done separately. Sections III, IV, and V are devoted to the development of an electromagnetic model for the core that is used in Sections VI and VII for the prediction of flux density distribution and power loss, respectively. In Section VIII a closed form expression for power loss is derived. Although this expression is not as accurate as the more detailed electromagnetic model developed Sections III, IV and V, it allows a quick assessment to be made on the relative importance of curvature related power loss. Section IX is about laboratory tests for the practical detection of power loss due to curvature related radial flux and Section X concludes the paper.

II. EDDY CURRENT LOSS SEPARATION

Induced currents within a lamination sheet are made up of the superposition of eddy currents due to flux that runs parallel to the lamination faces and eddy currents due to cross-lamination flux. Assume that the distribution of eddy currents due solely to a given distribution of parallel running flux is given by X. Similarly, assume that the distribution of eddy currents due solely to a given distribution of cross-lamination flux is given by Y. We now show that the power loss due to eddy current distribution X and that due to eddy current distribution Y are mutually independent and that interaction between the two eddy current distributions contribute zero net additional power loss. The power loss density, D, at any given point within a laminate is given by:

$$D = \frac{J_{rp}^2}{\sigma_r} + \frac{\left(J_{\theta c} + J_{\theta p}\right)^2}{\sigma_\theta} + \frac{\left(J_{zc} + J_{zp}\right)^2}{\sigma_z} \tag{1}$$

where the subscripts r, θ and z denote the radial, circumferential and axial directions, respectively, subscripts p and c relate to parallel running flux and cross-lamination flux, respectively, σ is the material conductivity and J is the induced current density.

Expansion of the right hand side of equation (1) gives:

$$D = \frac{J_{rp}^2}{\sigma_r} + \frac{J_{\theta p}^2}{\sigma_\theta} + \frac{J_{zp}^2}{\sigma_z} + \frac{J_{\theta c}^2}{\sigma_\theta} + \frac{J_{zc}^2}{\sigma_z} + \frac{2J_{\theta c}J_{\theta p}}{\sigma_\theta} + \frac{2J_{zc}J_{zp}}{\sigma_z} \qquad (2)$$

The first three terms of equation (2) represent contributions to power loss density coming from parallel running flux alone. The fourth and fifth terms represent contributions to power loss density coming from cross-lamination flux alone. The last two terms represent contributions to power loss density which result from the interaction between the two sets of induced currents. The following assumptions are now made:

a) $J_{\theta c}$ and J_{zc} are constant along a radial line within a laminate; and

b) If x is measured radially from the laminate centre, as shown in Figure 1, then, $J_{\theta p}(x)$ is equal to $-J_{\theta p}(-x)$ and $J_{zp}(x)$ is equal to $-J_{zp}(-x)$.

Based on these assumptions, it is clear that the last two terms in equation (2) do not contribute to the total power loss in the lamination.

The decoupling between power loss due to the parallel running flux and that due to cross-lamination flux allows them to be calculated separately. There are well established methods for the calculation of power loss due to parallel running flux [8] and these are applicable to laminated cores of axial flux machines. In this paper we consider only the power loss due to cross-lamination flux. Although cross-lamination

and parallel running flux are both present in the adopted model, eddy currents due to the latter have been eliminated by assuming zero radial conductivity. Whilst this assumption makes power loss due to parallel running flux equal to zero, it has no effect on the power loss due to cross-lamination flux.

III. Problem Formulation

The following simplifying assumptions are made:

a) Magnetic saturation and hysteresis are negligible.

b) Induced eddy currents do not have a radial component.

c) Permeabilities in the radial, axial and circumferential directions may differ, but are constants.

d) The core is considered solid rather laminated. However a much lower radial permeability is used to account for the lower permeability of the electrical insulation between laminations [9].

e) The core surface on the air-gap side is smooth, that is the effects of teeth and slots are ignored.

f) Flux enters the core from the air-gap side axially, with a sinusoidal variation in the circumferential direction.

g) The regions outside the core have zero permeability.

h) The quasi-static approximation to Maxwell's equations is applicable.

Based on assumption h) we can write:

$$\nabla \cdot \vec{B} = 0 \tag{3}$$

$$\nabla \times \vec{H} = \vec{J} \tag{4}$$

$$\nabla \times \vec{E} = -\frac{\partial \vec{B}}{\partial t} \tag{5}$$

$$\nabla \cdot \vec{J} = 0 \tag{6}$$

where $\vec{B}$ is the magnetic flux density, $\vec{H}$ the magnetic field intensity, $\vec{E}$ the electric field intensity and $\vec{J}$ is the current density.

The assumed constitutive relationships for the core are:

$$\vec{B} = \mu \vec{H} \tag{7}$$

and

$$\vec{J} = \sigma \vec{E}\,, \tag{8}$$

where

$$\mu = \begin{bmatrix} \mu_r & 0 & 0 \\ 0 & \mu_\theta & 0 \\ 0 & 0 & \mu_z \end{bmatrix}, \tag{9}$$

and

$$\sigma = \begin{bmatrix} 0 & 0 & 0 \\ 0 & \sigma_\theta & 0 \\ 0 & 0 & \sigma_z \end{bmatrix}. \tag{10}$$

We have chosen to adopt the $T - \Omega$ formulation [10]. The solenoidal condition of equation (6) allows $\vec{J}$ to be defined by

$$\vec{J} = \nabla \times \vec{T} \tag{11}$$

where $\vec{T}$ is the electric vector potential. Combining equations (4) and (11) we have

$$\nabla \times \left(\vec{H} - \vec{T} \right) = 0\,. \tag{12}$$

Equation (12) allows $\left(\vec{H} - \vec{T} \right)$ to be defined by

$$\left(\vec{H} - \vec{T} \right) = -\nabla \Omega \tag{13}$$

where Ω is the magnetic scalar potential. From equations (3), (7) and (13) we get

$$\nabla \cdot \mu \vec{T} - \nabla \cdot \mu \nabla \Omega = 0\,. \tag{14}$$

Using equations (5), (7), (8), (11) and (13) we can write

$$\nabla \times \sigma^{-1} \nabla \times \vec{T} = -j\omega\mu\left(\vec{T} - \nabla\Omega\right) \tag{15}$$

where the time derivative has been replaced by the $j\omega$ operator since analysis is restricted to the sinusoidal case at steady-state.

Assumption b) implies that $\vec{J}$ does not have any radial component and thus the axial and circumferential components of the vector $\vec{T}$ can be chosen to be zero.

Substituting equation (9) into (14) and expanding gives

$$\mu_r \frac{\partial^2\Omega}{\partial r^2} + \frac{\mu_r}{r}\frac{\partial\Omega}{\partial r} + \frac{\mu_\theta}{r^2}\frac{\partial^2\Omega}{\partial\theta^2} + \mu_z \frac{\partial^2\Omega}{\partial z^2} - \mu_r \frac{\partial T}{\partial r} - \mu_r \frac{T}{r} = 0. \tag{16}$$

By equating the radial components on the left and right hand sides of equation (15) and substituting equations (9) and (10) we obtain

$$j\omega\mu_r \frac{\partial\Omega}{\partial r} - j\omega\mu_r T + \frac{1}{\sigma_z r^2}\frac{\partial^2 T}{\partial\theta^2} + \frac{1}{\sigma_\theta}\frac{\partial^2 T}{\partial z^2} = 0\,. \tag{17}$$

It is possible to obtain another two equations by equating the circumferential and axial components of equation (15), respectively, however this is not necessary as there are only the two unknowns T and Ω. These two unknowns will be fully defined through equations (16), (17) and the imposed boundary conditions.

We now simplify equations (16) and (17) using the periodicity condition of assumption f). The sinusoidal variation in the imposed magnetic flux density at the core surface will result is the same behaviour for both T and Ω. Therefore:

$$\frac{\partial^2\Omega}{\partial\theta^2} = -\left(\frac{p}{2}\right)^2 \Omega \tag{18}$$

$$\frac{\partial^2 T}{\partial\theta^2} = -\left(\frac{p}{2}\right)^2 T\,, \tag{19}$$

where p in the number of machine poles. Substituting equation (18) into equation

(16) results in

$$\mu_r \frac{\partial^2 \Omega}{\partial r^2} + \frac{\mu_r}{r}\frac{\partial \Omega}{\partial r} - \frac{\mu_\theta}{r^2}\left(\frac{p}{2}\right)^2 \Omega + \mu_z \frac{\partial^2 \Omega}{\partial z^2} - \mu_r \frac{\partial T}{\partial r} - \frac{\mu_r}{r} T = 0 \tag{20}$$

and substituting equation (19) into (17) gives

$$j\omega\mu_r \frac{\partial \Omega}{\partial r} - j\omega\mu_r T - \frac{1}{\sigma_z r^2}\left(\frac{p}{2}\right)^2 T + \frac{1}{\sigma_\theta}\frac{\partial^2 T}{\partial z^2} = 0 \tag{21}$$

Based on assumptions f) and g) the imposed boundary conditions are such that the normal derivative of Ω is zero at all surfaces except at the air-gap boundary where

$$\frac{\partial \Omega}{\partial z} = \hat{B}_z(r)\cos\left(\frac{p\theta}{2}\right). \tag{22}$$

It is now possible to solve for T and Ω using equations (20) , (21) and the imposed boundary conditions. From the solution, the power loss due to induced eddy currents can be found.

IV. NUMERICAL SOLUTION

In principle any numerical technique could be used to solve for the fields inside the core. An attempt was made to solve the full 3D problem on a PC using commercially available finite element software. This was without success because of memory requirements. By taking advantage of the problem periodicity in the circumferential direction (see equations (18) and (19)) the problem can be reduced to one that is effectively two dimensional. The axiperiodic formulation is however not commonly available in commercial finite element packages. For this reason code has been

specifically written to solve this problem. The finite difference method was chosen because of its suitability and simplicity when the problem's geometry is simple.

The core is discretised as shown in Figure 2. The discretised plane is chosen to be a pole centre plane along which the angular coordinate θ is equal to zero. The plane contains $e_r \times e_z$ elements, where e_r is the number of divisions in the radial direction and e_z the number of divisions in the axial direction. An element centred at radius r_i, has a volume given by $\Delta r \Delta z\, r_i d\theta$ where $d\theta$ is infinitely small. A node is assumed to exist at the centroid of each element. The location of a node is identified by three subscripts i, j and k which increment in the positive radial, circumferential and axial directions, respectively. Node $(1,1,1)$ is located at $(R_i + \Delta r/2, 0, \Delta z/2)$. The node location index j and explicit reference to the dimension $d\theta$ of the elements are not essential, but are included for ease of physical interpretation. Subscripts i, j, k when used with $\boldsymbol{\Omega}$ and $\boldsymbol{T}$ indicate values of those quantities at node (i, j, k). The discretised form of equations (20) and (21) are derived in Appendix A. Application of those at all nodes results in the following matrix equation:

$$\left[\begin{array}{c|c} \mathbf{P} & \mathbf{Q} \\ \hline j\omega\mathbf{W} & \mathbf{R} + j\omega\mathbf{S} \end{array}\right]\left[\begin{array}{c} \boldsymbol{\Omega} \\ \hline \mathbf{I} \end{array}\right] = \left[\begin{array}{c} \boldsymbol{\Phi} \\ \hline \mathbf{0} \end{array}\right] \tag{23}$$

where $\mathbf{P}$ is an $(e_r e_z)\times(e_r e_z)$ matrix of permeances, $\mathbf{Q}$ is an $(e_r e_z)\times((e_r - 1)e_z)$ matrix of permeances, $\mathbf{W}$ is an $((e_r - 1)e_z)\times(e_r e_z)$ matrix of permeances, $\mathbf{R}$ is an $((e_r - 1)e_z)\times((e_r - 1)e_z)$ matrix of resistances, $\mathbf{S}$ is an $((e_r - 1)e_z)\times((e_r - 1)e_z)$ matrix of permeances, $\boldsymbol{\Omega}$ is a vector of magnetic scalar potentials for node $(1,1,1)$

through to node $(e_r, 1, e_z)$, **I** is an $((e_r - 1)e_z) \times 1$ vector of induced currents and **Φ** is an $(e_r e_z) \times 1$ vector of imposed flux. The elements of vector **I** are given by

$$I_{i,j,k} = \frac{(T_{i,j,k} + T_{i+1,j,k})\Delta r}{2}. \tag{24}$$

Current $I_{i,j,k}$ is effectively a loop current that exists around a reluctive branch between nodes (i, j, k) and $(i+1, j, k)$. The assumption of zero conductivity in the radial direction restricts the existence of those loop currents around radial reluctive branches only.

Expressions for the evaluation of entries for **P**, **Q**, **W**, **R** and **S** are derived in the appendix in terms of physical dimensions and material properties. The appendix also provides expressions for the elements of **Φ** in terms of the imposed boundary conditions. Values for vectors **Ω** and **I** are found by solving equation (23). From these values the magnetic flux density at any point in the core and the power loss due to induced currents can be evaluated.

V. Power Loss Calculation

In terms of the electric vector potential, power loss density D is given by

$$D = \frac{1}{\sigma_\theta}\left(\frac{\partial T}{\partial z}\right)^2 + \frac{1}{\sigma_z r^2}\left(\frac{\partial T}{\partial \theta}\right)^2. \tag{25}$$

For the axiperiodic case

$$T = \hat{T}(r, z)\cos\left(\frac{p\theta}{2}\right) \tag{26}$$

where $\hat{T}(r, z)$ is the peak value of T on a pole-centre plane. Substituting equation (26) into (25) gives

$$D = \frac{1}{\sigma_\theta}\left(\frac{\partial \hat{T}}{\partial z}\right)^2 \cos^2\left(\frac{p\theta}{2}\right) + \frac{1}{\sigma_z r^2}\left(\frac{p}{2}\right)^2 \hat{T}^2 \sin^2\theta \,. \tag{27}$$

Equation (24) allows T within the half of any element between r_i and $r_i + \Delta r/2$ to be approximated as $I_{i,j,k}/\Delta r$, and similarly, in the other half T can be approximated as $I_{i-1,j,k}/\Delta r$.

Based on the above arguments, we arrive at equation (28) which is an expression for the core power loss, F, due to the induced currents.

$$F = \frac{\pi}{2}\sum_{i=1}^{e_r}\sum_{k=1}^{e_z}\left(\frac{p}{2}\right)^2 \frac{\left(I_{i,j,k}^2 + I_{i-1,j,k}^2\right)\Delta z}{2\sigma_z r_i \Delta r} + r_i\left[\frac{\left(I_{i,j,k+1} - I_{i,j,k-1}\right)^2 + \left(I_{i-1,j,k+1} - I_{i-1,j,k-1}\right)^2}{4\sigma_\theta \Delta z \Delta r}\right] \tag{28}$$

where

$$\begin{aligned}
&j = 1 \\
&I_{i-1,j,k} = I_{i-1,j,k+1} = I_{i-1,j,k-1} = 0 \quad \text{if} \quad i = 0 \\
&I_{i,j,k} = I_{i,j,k+1} = I_{i,j,k-1} = 0 \qquad \text{if} \quad i = e_r \\
&I_{i,j,k-1} = I_{i-1,j,k-1} = 0 \qquad \text{if} \quad k = 1 \\
&I_{i,j,k+1} = I_{i-1,j,k+1} = 0 \qquad \text{if} \quad k = e_z
\end{aligned}$$

and all other values of I are obtained by solving equation (23).

The above expression for power loss is for the case where the fields are stationary with respect to the core and pulsating at frequency ω. That is $B(r,\theta,t)$ in equation (22) is given by $\hat{B}_z(r)\cos(\omega t)\cos(p\theta/2)$. In practice, a rotating air-gap magnetic field is more likely, in which case

$$B_z(r,\theta,t) = \hat{B}_z(r)\cos(\omega t - p\theta/2). \tag{29}$$

It can be shown that, for any given $\hat{B}_z(r)$, the power loss for the rotating field case is twice that for the pulsating field.

VI. Theoretical Prediction: Flux Density distribution

The model developed in Sections III, IV and V has been used to analyse the flux density distribution in a core with the following nominal characteristics: $R_i = 0.075\text{m}$, $R_o = 0.175\text{m}$, $L = (0.2/\text{p})\text{m}$, $\mu_r = 20\mu_o$, $\mu_\theta = 1000\mu_o$, $\mu_z = 1000\mu_o$, $\sigma_r = 0$, $\sigma_\theta = 5\times10^6\text{S/m}$, $\sigma_z = 5\times10^6\text{S/m}$, $\omega = 100\pi$ and $\hat{B}_z = 0.7\,\text{T}$. In practice it would be expected that the core back-iron length *L* will be progressively reduced as the number of poles is increased. For this reason the length of the back-iron has been chosen be inversely proportional to the number of poles. Figure 3 shows theoretical predictions for the normalised radial flux density as a function of radius, and averaged over the core axial length. Similarly, Figure 4 shows the normalised circumferential flux density as a function of radius, averaged over the core axial length.

The following observations can be made:

a) The peak radial flux density is much smaller than the peak axial or circumferential flux densities.
b) The radial flux density is almost non-existent under a.c. conditions. This is theoretical confirmation of what was already postulated in reference [7] based on magnetostatic analysis and experimental results.
c) The amount of radial flux, although small, is a strong function of core permeability.

d) The circumferential flux density is greatest near the outer radius of the core. As stated in [7], this must be accounted for when sizing the back-iron of axial flux machines.

VII. Theoretical Prediction: Power Loss

The core model has also been used to make predictions of power loss due to cross-lamination flux. The assumed nominal core characteristics are the same as those of Section VI. Power loss predictions are shown in Table 1 and Figure 5.

For comparison, classical eddy-current power losses due to parallel flux, F_p, have been evaluated using

equation (30) [8].

$$F_p = \frac{\omega^2 \sigma t^2}{24} \int_V \left| B(r,\theta,z) \right|^2 \partial V \qquad (30)$$

where t is the laminate thickness (= 0.27mm) and V the core volume. These values are shown in Table 2.

The following observations can be made:

a) There is a strong dependence of power loss F on the number of poles and on the relative permeability of the core.

b) Except for the two-pole case and at low values of core permeability, the power loss due to cross-lamination flux is insignificant compared to the power loss due to parallel flux.

c) The power loss due to cross-lamination flux may be expressed as:

$$F = k\sqrt{f} \qquad (31)$$

where k is independent of frequency but is a function of physical dimensions, material properties, number of poles and $\hat{B}_z(r)$. Good fits to the curves in Figure 5

are obtained with k chosen to be 0.2285 and 0.0691 for the 2- and 4- pole cases, respectively.

The explanation for observation c) is based on characteristics of the circumferential component of the induced current which is shown in Figures 6 and 7. The first point is that the induced current experiences high resistance circumferentially since it is restricted to flow through a thin layer near the flat surfaces of the core because of the skin-effect. The second point is that the total circumferential current (Figure 7) is practically independent of frequency. The high circumferential resistance, compared to the axial resistance, implies that practically all the power losses are associated with the circumferential component of current. Thus we have a current, which is itself almost independent of frequency, flowing through a cross-sectional area that is proportional to the skin-depth. This implies that the power loss is proportional to the square root of frequency.

VIII. CLOSED FORM EXPRESSION FOR POWER LOSS

It was shown in Section VII that the relative significance of power loss due to cross lamination flux depends on several factors including the number of poles, material properties physical dimensions and operating frequency. The closed form expression , which is now derived, can be used by axial flux machine designers to make quick assessments on the requirement to consider power loss due to cross lamination flux. As shown in Figure 8, the core is represented by a simplified equivalent coupled reluctive-resistive network. The reluctive circuit contains only three nodes. Nodes A and B are located on the pole centre plane at $\left(R_i + \left(R_o - R_i\right)/4, 0, L/2\right)$ and

$\left(R_o - \left(R_o - R_i\right)/4, 0, L/2\right)$, respectively. The third node represents the plane of uniform magnetic potential which is equidistant from adjacent pole centre planes. The resistive circuit is a single loop linking the reluctive branch which represents permeance in the radial direction between nodes A and B. The following assumptions are made:

a) Half of the flux per pole that enters the core from the air-gap between $r = R_i + \left(R_o - R_i\right)/2$ and $r = R_o$ flows through branch BO. This is represented by ϕ_{out} in Figure 8.

b) Half of the flux per pole that enters the core from the air-gap between $r = R_i$ and $r = R_i + \left(R_o - R_i\right)/2$ flows through branch AO. This is represented by ϕ_{in} in Figure 8.

c) The resistance of the resistive loop is sufficiently small such that the induced current cause the net flux flowing in the reluctive branch between nodes A and B to be practically zero.

d) Reluctance in the axial direction is assumed to be zero.

e) Branch BO represents flux paths between $r = R_i + \left(R_o - R_i\right)/2$ and $r = R_o$.

f) Branch AO represents flux paths between $r = R_i$ and $r = R_i + \left(R_o - R_i\right)/2$.

g) Due to the skin effect, the circumferential component of the loop current decays exponentially from the core flat surfaces with characteristic decay length equal to the skin depth.

Equations (32) to (40) are based on the above assumptions.

$$P_{\text{out}} = \frac{2p\mu_\theta L\left(R_o - R_i\right)}{\pi\left(3R_o + R_i\right)} \tag{32}$$

$$P_{\text{in}} = \frac{2p\mu_\theta L\left(R_o - R_i\right)}{\pi\left(3R_i + R_o\right)} \tag{33}$$

$$\phi_{\text{out}} = \frac{\hat{B}_z \left(3R_o + R_i\right)\left(R_o - R_i\right)}{4p} \tag{34}$$

$$\phi_{\text{in}} = \frac{\hat{B}_z \left(3R_i + R_o\right)\left(R_o - R_i\right)}{4p} \tag{35}$$

$$R_z = \frac{2pL}{\sigma_z \pi \left(R_o^2 - R_i^2\right)} \tag{36}$$

where R_z is the axial component of the loop resistance,

$$R_\theta = \frac{\pi \left(R_o + R_i\right)}{\sigma_\theta p \delta \left(R_o - R_i\right)} \tag{37}$$

where R_θ is the circumferential component of the loop resistance and δ is the skin depth given by

$$\delta = \sqrt{\frac{2}{\omega \mu_r \sigma_\theta}} \tag{38}$$

$$\begin{aligned} I &= \text{loop current} \\ &= \Omega_{\text{out}} - \Omega_{\text{in}} \\ &= \frac{\phi_{\text{out}}}{P_{\text{out}}} - \frac{\phi_{\text{in}}}{P_{\text{in}}} \\ &= \frac{\hat{B}_z \pi \left(R_o^2 - R_i^2\right)}{\mu_\theta L p^2} \end{aligned} \tag{39}$$

$$\begin{aligned} F &= 2pI^2 \left(R_z + R_\theta\right) \\ &= \frac{\hat{B}_z{}^2 \pi^2 \left(R_o^2 - R_i^2\right)}{\mu_\theta^2 L^2 p^3} \left[\frac{2pL}{\pi \sigma_z} + \frac{\pi \left(R_o + R_i\right)^2}{p \delta \sigma_\theta} \right] \end{aligned} \tag{40}$$

Table 3 compares predictions based on the axiperiodic model with those found using equation (40). It shows that equation (40) tends to over estimate power loss by up to a factor of 2. This is still reasonable since equation (40) is based on fairly crude assumptions. The nature of those assumptions is such that they lead to an overestimation of power loss. Although the predictions made by equation (40) are not

very accurate, it can still be used by machine designers to allow a quick decision to be made on whether or not there is a need for detailed investigation into power loss due cross-lamination flux.

IX. Laboratory Tests

The theory that has been presented points to the possibility of increased core loss due to the curvature of the core in axial flux machines. Curvature related loss cannot be separately measured as it is part of the total input power to the machine. Its extraction from total measured core loss could, however, be based on its relationship with frequency. Total core loss, P_T, could be expressed as

$$P_T = F + k_1 f + k_2 f^{3/2} + k_3 f^2 \tag{41}$$

where F represents loss due to cross-lamination flux, $k_1 f$ represents hysteresis loss, $k_2 f^{3/2}$ represents excess loss [11][12] and $k_3 f^2$ represents classical eddy-current loss due to parallel running flux.

As shown in Figure 9, if there is a significant amount of eddy current loss due to cross-lamination flux, then the axiperiodic model predicts a non-linear relationship between P_T / f and f. The non-linearity is characterised by a minimum point occurring at frequency f_m. The more significant the loss due to cross-lamination flux is, compared to normal eddy current loss, the higher the value of f_m and the easier it would be to locate using test data. The practical identification of the turning point at f_m requires tests to be performed over a frequency range extending sufficiently below f_m. Indication of the existence of a turning point by test data signifies the presence of a significant amount of power loss due to cross-lamination flux. Conversely, it can be

shown that if F is equal to zero, no turning point exists in the P_T / f against f graph. Equation (42) which is obtained from equations (31) and (41), is now used to show how loss due to cross-lamination flux can be separated from the other core loss components.

$$\frac{P_T}{f} = \frac{k}{\sqrt{f}} + k_1 + k_2\sqrt{f} + k_3 f \tag{42}$$

By differentiating the right hand side of (42) and equating to zero we obtain

$$k = k_2 f_m + 2k_3 f_m^{3/2}. \tag{43}$$

It can also be shown that:

$$k = \frac{2\sqrt{f_m}\left(Q_n - Q_m\right) + k_2 f_m\left(3 - 2\sqrt{2}\right)}{\left(\sqrt{2} - 1\right)} \tag{44}$$

where Q_m and Q_n are defined in Figure 9. Equation (44) allows k to be estimated from experimental data. If accurate estimation of k_2 is not possible, and it is assumed to be zero (k_3 assuming its maximum possible value), equation (44) returns the lower bound for k. Equation (45), which is based on the assumption of k_3 being equal to zero (k_2 assuming its maximum possible value), gives the upper bound for k.

$$k = \frac{\sqrt{2 f_m}\left(Q_n - Q_m\right)}{\left(3 - 2\sqrt{2}\right)} \tag{45}$$

By comparing equations (44) and (45), it can be deduced that the maximum error from assuming a zero value for k_2 in equation (44) is 41%. However, such a high error is unlikely in practice as classical eddy-current loss will always be relatively significant compared to excess loss.

Figure 11 shows experimental data for test cores with the same physical dimensions as those given in Section VI. The experimental set-up is shown in Figure 10. Core loss, for both cores, was obtained by subtracting copper loss from the measured power. The experimental results suggest that core loss due to cross-lamination flux is not significant. That is, there is no indication of the existence of a turning point as test frequency falls. From measurements made with one of the cores wound as a toroidal transformer, the core permeability was estimated to be greater than $5000\mu_o$. From the manufacturer's data σ_θ was estimated to be about 4.5×10^6 S/m. Based on these values the axiperiodic model predicts the losses due to cross-lamination flux to be 0.311W at 50Hz. This is relatively small compared to the total measured core loss of approximately 21W of which 10W is estimated to be hysteresis loss. It is not surprising, therefore, that the experimental data points in Figure 11 do not indicate the existence of a significant amount of power loss due to cross-lamination flux.

X. Conclusions

A model has been developed to evaluate the effect of curvature on flux density distribution and power loss in laminated cores of axial flux machines. It has been found that, compared to the peak flux density in the axial or circumferential direction, the flux density in the radial direction is negligible. Consequently the circumferential flux density in the back-iron, averaged over the axial length, is proportional to radius. Laminations near the outer radius are subject to higher circumferential flux densities compared to laminations near the inner radius. Designers should take this into consideration when sizing the core back-iron.

The tendency for flux to flow in the radial direction creates an additional component of power loss due to eddy currents. The significance of this component is strongly dependent on the number of poles, core permeability and core conductivity. It has been found that if the core permeability, core conductivity and number of poles are high enough $\left(\mu > 1000\mu_o, \sigma > 10^6, p > 2\right)$ then power loss due to curvature related cross-lamination flux is negligible compared to normal eddy current losses. A closed form expression has been derived to help machine designers make a quick assessment on whether or not power losses due curvature related radial flux is likely to be significant. If that is the case, the more detailed axiperiodic model presented here can be used to predict the losses. Direct measurement of this power loss is not possible. However, if values of total core loss are obtainable from tests, then, the component of power loss due cross-lamination flux can be isolated based on its frequency dependence.

REFERENCES

[1] Varga, J. S.: 'Magnetic and Dimensional Properties of Axial Induction Motors', *IEEE Trans. Energy Convers.*, June 1986, **EC-1**, (2), pp. 137-144.

[2] Chan, C. C.: 'Axial-Field Electrical Machines – Design and Applications', *IEEE Trans. Energy Convers.*, June 1987, **EC-2**, (2), pp. 294-300.

[3] Zhang, Z., Profumo, F., and Tenconi, A.: 'Axial-flux versus radial-flux permanent-magnet motors', *Electromotion,* 1996, **3**, pp. 134-140.

[4] Zhilichev, Y. N.: 'Three-Dimensional Analytic Model of Permanent Magnet Axial Flux Machine', *IEEE Trans. Mag.*, Nov. 1998, **34**, (6), pp. 3897-3901.

[5] Bumby, J. R., Martin, R. , Mueller, M. A. , Spooner, E. , Brown, N. L. and Chalmers, B. J.: 'Electromagnetic design of axial-flux permanent magnet machines', *IEE Proc., Electr. Power Appl.*, March. 2004, **151**, (2), pp. 151-160.

[6] Boldea, I., Rahman, A., and Nasar, S. A.: 'Finite-Width, Finite-Thickness, and Saturation Effects in Solid-Rotor Induction Machines', *IEEE Trans. Power Appar. Syst.*, Sept.-Oct. 1975, **PAS-94**, (5), pp. 1500-1507.

[7] Hewitt, A. J., Ahfock, T., and Suslov, S. A.: 'Magnetic Flux Density Distribution in Axial Flux Machine Cores', *IEE Proc. Electr. Power Appl.*, March 2005, **152**, (2), pp. 292-296.

[8] Lammeraner, J., and Stafl, M.: 'Eddy currents' (ILIFFE Books Ltd., London, 1966)

[9] Reece, A. B. J., and Preston, T. W.: 'Finite Element Methods in Electrical Power Engineering' (Oxford University Press Inc., New York, 2000)

[10] Ratnajeevan S., and Hoole H. (Editors), 'Finite Elements, Electromagnetics and Design' (Elsevier Science B.V., Amsterdam, 1995)

[11] Barbisio, E., Fiorillo, F., and Ragusa, C.: 'Predicting Loss in Magnetic Steels Under Arbitrary Induction Waveform and with Minor Hysteresis Loops' *IEEE Trans. Mag.*, July 2004, **40**, (4), pp. 1810-1819.

[12] Fiorillo F., and Novikov, A.: 'An Improved Approach to Power Losses in Magnetic Laminations under Nonsinusoidal Induction Waveform' *IEEE Trans. Mag.*, Sept. 1990, **26**, (5), pp. 2904-2910.

APPENDIX A

The purpose of this appendix is to derive expressions to evaluate the entries for matrices **P**, **Q**, **W**, **R**, **S** and **Φ**.

For each node (i, j, k), if k is greater than 1, equation (20) yields

$$\mu_r\left[\frac{2\Omega_{i,j,k}-\Omega_{i-1,j,k}\left(r_i-\Delta r/2\right)/r_i-\Omega_{i+1,j,k+1}\left(r_i+\Delta r/2\right)/r_i}{\Delta r^2}\right]$$
$$+\mu_z\left[\frac{2\Omega_{i,j,k}-\Omega_{i,j,k-1}-\Omega_{i,j,k+1}}{\Delta z^2}\right]+\mu_r\frac{\left(T_{i,j,k}+T_{i+1,j,k}\right)\left(r_i+\Delta r/2\right)}{2r_i\Delta r} \qquad \text{(A1)}$$
$$+\mu_\theta\left(\frac{p}{2}\right)^2\frac{\Omega_{i,j,k}}{r_i^2}-\mu_r\frac{\left(T_{i-1,j,k}+T_{i,j,k}\right)\left(r_i-\Delta r/2\right)}{2r_i\Delta r}=0.$$

For each node (i, j, k), if k is equal to 1, then equation (20) yields

$$\mu_r\left[\frac{2\Omega_{i,j,k}-\Omega_{i-1,j,k}\left(r_i-\Delta r/2\right)/r_i-\Omega_{i+1,j,k+1}\left(r_i+\Delta r/2\right)/r_i}{\Delta r^2}\right]$$
$$+\mu_z\left[\frac{\Omega_{i,j,k}-\Omega_{i,j,k+1}}{\Delta z^2}\right]+\mu_r\frac{\left(T_{i,j,k}+T_{i+1,j,k}\right)\left(r_i+\Delta r/2\right)}{2r_i\Delta r} \qquad \text{(A2)}$$
$$+\mu_\theta\left(\frac{p}{2}\right)^2\frac{\Omega_{i,j,k}}{r_i^2}-\mu_r\frac{\left(T_{i-1,j,k}+T_{i,j,k}\right)\left(r_i-\Delta r/2\right)}{2r_i\Delta r}=\frac{\hat{B}_z\left(r_i\right)}{\Delta z}.$$

Application of equations (A1) and (A2) to all nodes results in the following matrix equation

$$\mathbf{P\Omega}+\mathbf{QI}=\mathbf{\Phi}. \qquad \text{(A3)}$$

$P(m,n)$ is non-zero only if m is equal to n or if nodes m and n are adjacent to each other. If node n is adjacent to node m in the axial direction then

$$P(m,n)=P(n,m)=-\frac{\mu_z r_i\Delta r}{\Delta z}. \qquad \text{(A4)}$$

$-P(m,n)\,d\theta$ could be regarded as the permeance in the axial direction across adjacent halves of neighbouring elements located at radius r_i. If node n is adjacent to node

m in the radial direction, then

$$P(m,n) = P(n,m) = -\frac{\mu_r \Delta z (r_i \pm \Delta r/2)}{\Delta r}. \tag{A5}$$

Here, $-P(m,n)d\theta$ could be regarded as the permeance in the radial direction across adjacent halves of neighbouring elements, one with centre at radius r_i and the other with centre at radius $r_i \pm \Delta r$. If $m = n$, then

$$P(m,m) = \left(\frac{p}{2}\right)^2 P_c - \sum_{\substack{j=1 \\ j \neq m}}^{e_r e_z} P(m,j), \tag{A6}$$

where

$$P_c = \frac{\mu_\theta \Delta r \Delta z}{r_i}. \tag{A7}$$

The expression $P_c / d\theta$ could be regarded as the permeance in the circumferential direction across adjacent halves of neighbouring elements located at radius r_i. The factor $(p/2)^2$ arises from the relationship between $\Omega(\theta)$ and $\Omega(\theta + d\theta)$.

It can be deduced from equations (A1) and (A2) that $Q(m,q)$ is zero unless node m and loop q are adjacent to each other in the radial direction, in which case

$$Q(m,q) = \frac{\mu_r \Delta z (r_i + \Delta r/2)}{\Delta r} \tag{A8}$$

for node m at radius r_i and loop q between radii r_i and $r_i + \Delta r$, or

$$Q(m,q) = -\frac{\mu_r \Delta z (r_i - \Delta r/2)}{\Delta r} \tag{A9}$$

if node m is at radius r_i and loop q between radii r_i and $r_i - \Delta r$.

$\Phi(m)$ is zero for all nodes except those directly facing the air-gap, in which case

$$\Phi(m) = \hat{B}_z(r_i) r_i \Delta r. \tag{A10}$$

$\Phi(m)d\theta$ may be regarded as the flux entering the element facing the air-gap and located at radius r_i.

For each loop current (i, j, k), defined by equation (24), equation (21) yields

$$
\begin{aligned}
&-j\omega\mu_r \frac{\left(\Omega_{i+1,j,k}-\Omega_{i,j,k}\right)}{\Delta r}+j\omega\mu_r \frac{\left(T_{i,j,k}+T_{i+1,j,k}\right)}{2} \\
&+\frac{1}{\sigma_\theta}\frac{2\left(T_{i,j,k}+T_{i+1,j,k}\right)-\left(T_{i,j,k-1}+T_{i+1,j,k-1}\right)-\left(T_{i,j,k+1}+T_{i+1,j,k+1}\right)}{2\Delta z^2} \\
&+\frac{1}{\sigma_z}\left(\frac{p}{2}\right)^2 \frac{\left(T_{i,j,k}+T_{i+1,j,k}\right)}{2\left(r_i+\Delta r/2\right)^2}=0.
\end{aligned}
\tag{A11}
$$

Application of equation (A11) to all loops results in the matrix equation

$$j\omega\mathbf{W\Omega}+\left(\mathbf{R}+j\omega\mathbf{S}\right)\mathbf{I}=\mathbf{0}\,. \tag{A12}$$

It can be deduced from equation (A11) that $W(q,m)$ is zero unless node m and loop q are adjacent to each other in the radial direction, in which case

$$W(q,m)=\frac{\mu_r \Delta z\left(r_i+\Delta r/2\right)}{\Delta r} \tag{A13}$$

for node m at radius r_i and loop q between radii r_i and $r_i+\Delta r$, and

$$W(q,m)=-\frac{\mu_r \Delta z\left(r_i+\Delta r/2\right)}{\Delta r} \tag{A14}$$

if node m is at radius r_i and loop q is between radii r_i and $r_i-\Delta r$.

$R(q,u)$ is non-zero only if q is equal to u or if loops q and u are adjacent to each other and both lie between r_i and $r_i+\Delta r$. In this case:

$$R(q,u)=-\frac{\left(r_i+\Delta r/2\right)}{\sigma_\theta \Delta r \Delta z}\,. \tag{A15}$$

$-R(q,u)d\theta$ could be regarded as the resistance in the circumferential direction along

adjacent halves of neighbouring elements, centred at radii r_i and $r_i + \Delta r$, respectively. If $q = u$, then

$$R(q,q) = \left(\frac{p}{2}\right)^2 R_z - \sum_{\substack{j=1 \\ j \neq q}}^{e_z(e_r-1)} R(q,j) \tag{A16}$$

where

$$R_z = \frac{1}{\sigma_z}\left(\frac{p}{2}\right)^2 \frac{\Delta z}{\Delta r\left(r_i + \Delta r/2\right)}. \tag{A17}$$

$R_z/d\theta$ could be regarded as the resistance in the axial direction along adjacent halves of neighbouring elements, centred at radii r_i and $r_i + \Delta r$, respectively. The factor $(p/2)^2$ arises from the relationship between $I(\theta)$ and $I(\theta + d\theta)$.

It can be deduced from equation (A11) that $S(q,u)$ is non-zero only if q is equal to u, in which case, assuming loop q is located between radii r_i and $r_i + \Delta r$,

$$S(q,q) = \frac{\mu_r \Delta z\left(r_i + \Delta r/2\right)}{\Delta r}. \tag{A18}$$

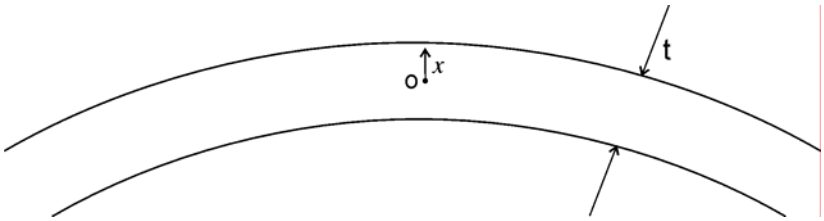

Figure 1. Cross-section of a lamination sheet.
0 = lamination centre, t = lamination thickness

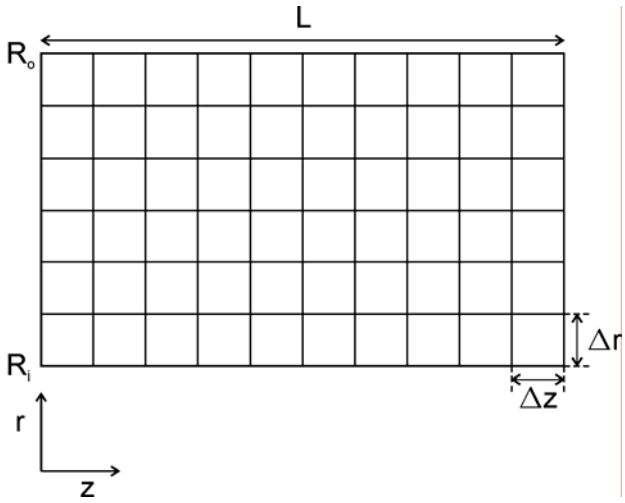

a) full plane

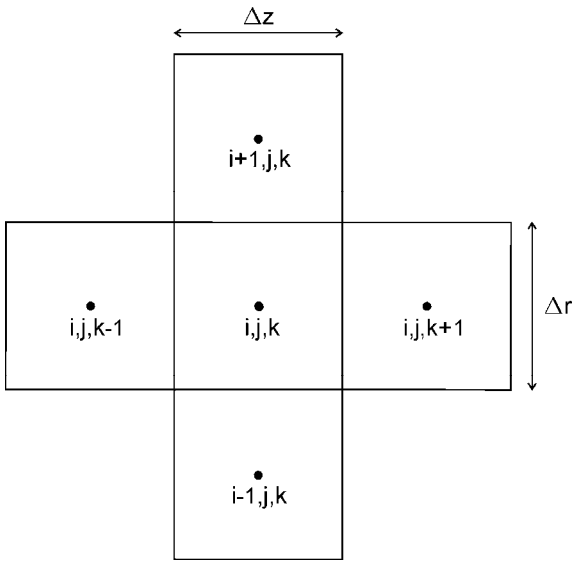

b) node location

Figure 2. Core discretisation along the plane $\theta = 0$.

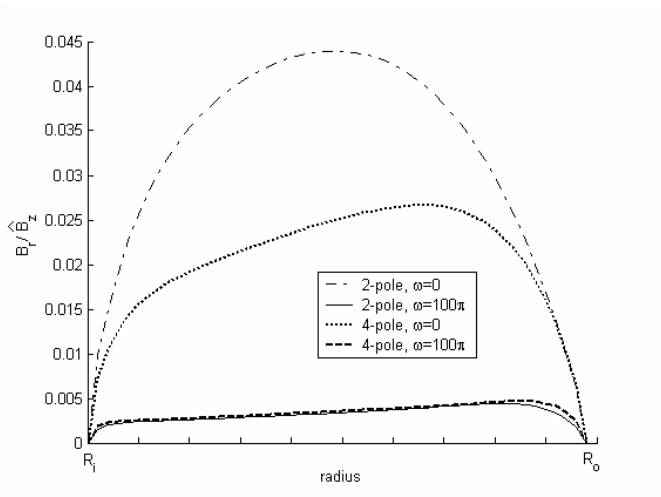

a) $\mu_\theta = \mu_z = 1000\mu_o$

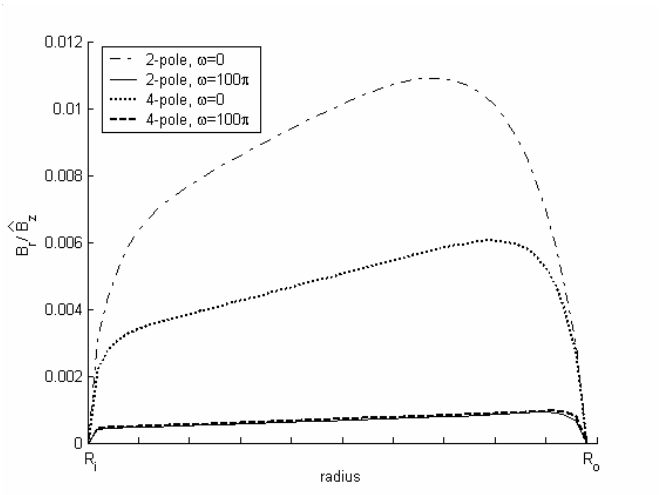

b) $\mu_\theta = \mu_z = 5000\mu_o$

Figure 3: Normalised average radial flux density along a pole-centre plane.

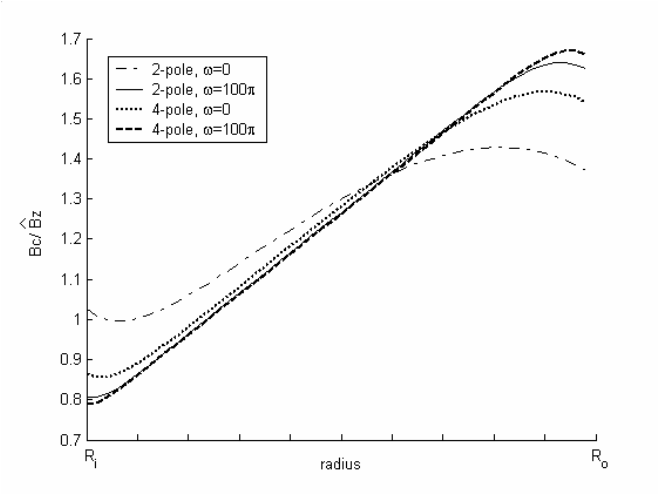

a) $\mu_\theta = \mu_z = 1000\mu_o$

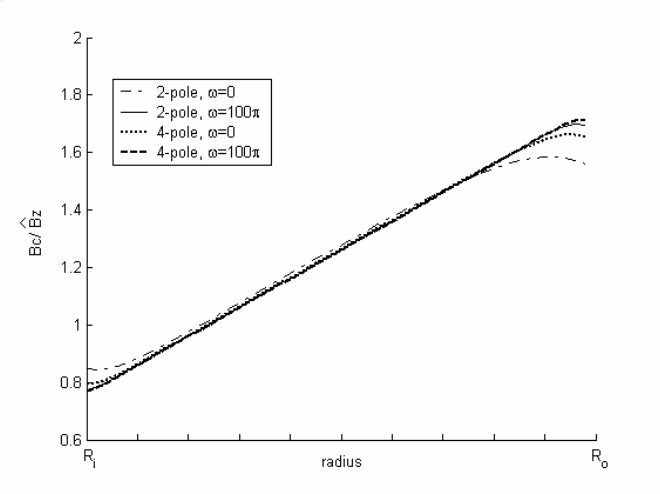

b) $\mu_\theta = \mu_z = 5000\mu_o$

Figure 4: Normalised average circumferential flux density half way between pole-centre planes.

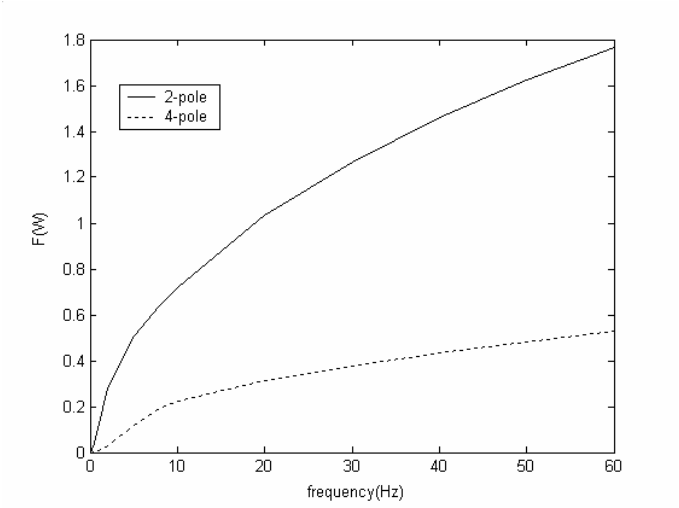

Figure 5: Dependence of power loss on frequency.

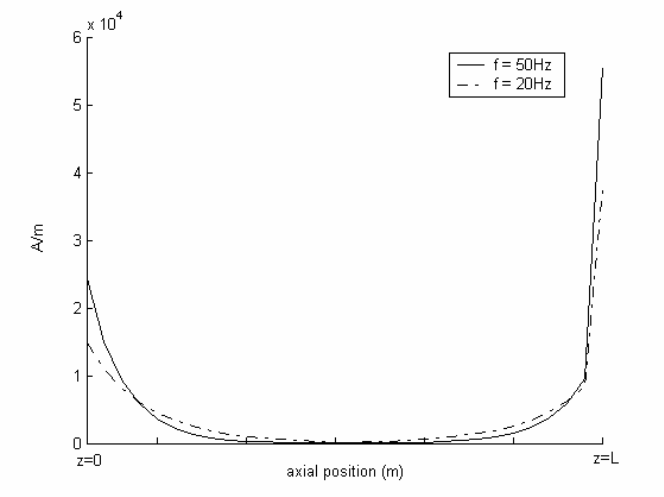

Figure 6: Circumferential current distribution (integrated from R_i to R_o) along a pole centre plane (2-pole machine).

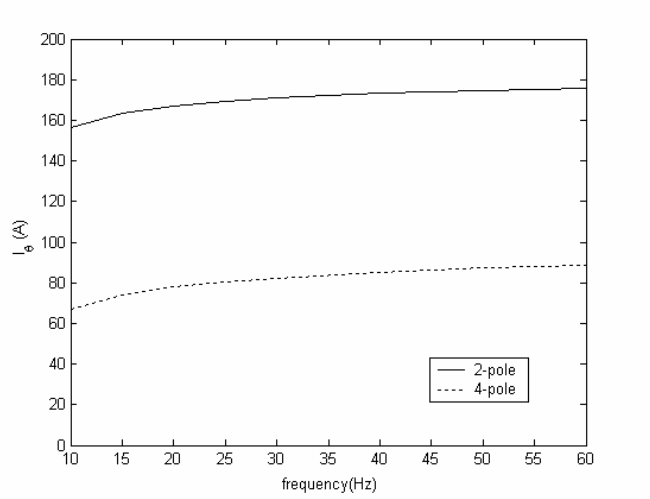

Figure 7: Circumferential current crossing the pole-centre plane in one direction.

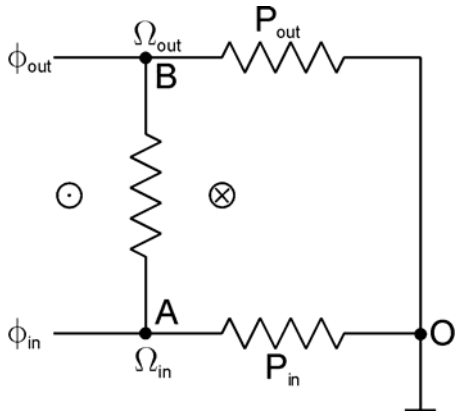

Figure 8: Simplified representation of the core.

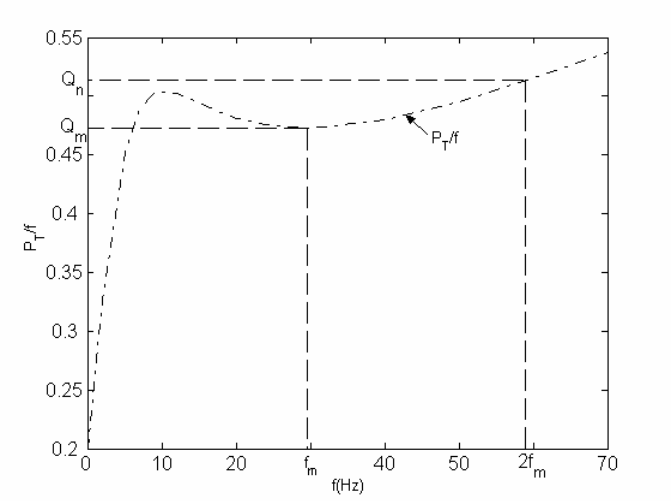

Figure 9: Calculation of *k* from experimental data.

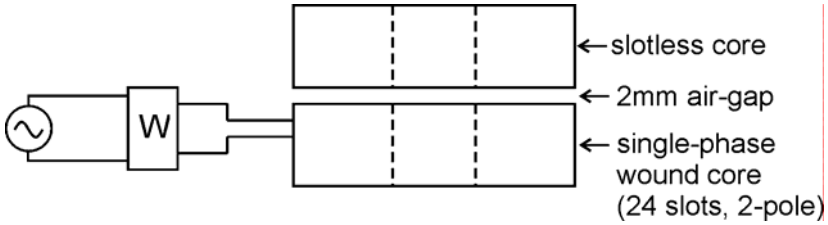

Figure 10: Experimental set-up for measuring core losses.

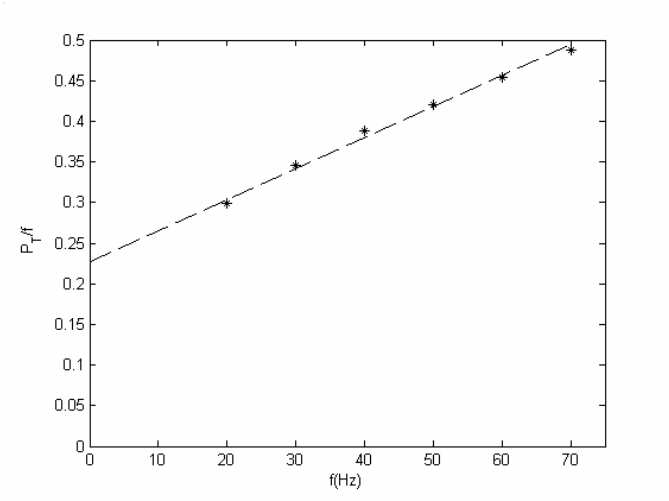

Figure 11: Experimental results ($\hat{B}_z = 0.5T$)

Table 1: Power losses due to cross-lamination flux

Number of poles	Losses (W) for $\mu = 1000\mu_o$	Losses (W) for $\mu = 5000\mu_o$
2	1.62	0.074
4	0.482	0.021
6	0.236	0.011
8	0.144	0.006

Table 2: Power losses due to parallel flux

Number of poles	2	4	6	8
$F_p(W)$	6.16	3.07	2.05	1.52

Table 3: Comparison between power loss (F) predicted by equation (40) and that predicted by the axiperiodic model.

Losses(W)	2-pole	4-pole	6-pole	8-pole
From equation (40)	2.66	0.672	0.308	0.171
From the axiperiodic formulation	1.62	0.482	0.236	0.144